J.L. Torero, "Material Properties that Control Ignition and Spread of a Fire in Micro-Gravity Environments," ASME Heat Transfer Conference, ASME-NHTC-2000-12314, 2000

Proceedings of NHTC'00
34th National Heat Transfer Conference
Pittsburgh, Pennsylvania, August 20–22, 2000

NHTC2000-12314

MATERIAL PROPERTIES THAT CONTROL IGNITION AND SPREAD OF A FIRE IN MICRO-GRAVITY ENVIRONMENTS

Jose L. Torero
Department of Fire Protection Engineering
University of Maryland
College Park, MD20742-3031
USA

ABSTRACT

A study of the different mechanisms controlling the initial stages of a fire in a micro-gravity environment is presented. Three different processes are deemed important for evaluation of material flammability, piloted ignition, co-current and counter-current flame spread. The three processes are evaluated in terms of thermal theory and the different material properties controlling these combustion processes are extracted. Experimental results obtained from ground testing, drop towers, parabolic flights and sounding rocket experiments serve to validate the present approach.

INTRODUCTION

The necessary flammability requirements for all materials to be used in space vehicles (NASA specifications) are given by the "Flammability, Odor, Offgassing, and Compatibility Requirements and Test Procedures for Materials in Environments that Support Combustion" document [1]. This document specifies two test that need to be performed before a material is qualified to be used in a space vehicle, the "Upward Flame Propagation Test" (Test 1) and the "Heat and Visible Smoke Release Rates Test" (Test 2). These two tests are expected to properly assess the flammability of a material in micro-gravity conditions. The basic principle behind these two test methods is an attempt to provide a worst case scenario (Test 1) and a measure of the heat release (Test 2), and consequently, the "damage potential" of a fire. A detailed description of these test methods is provided in NASA-NHB 8060.1 [1] and an extensive list of the materials that have been tested is provided in the "Materials Selection List for Space Hardware Systems" [2]. Background information for Test 2 is summarized in reference [3].

A general overview of fire safety practices is provided by Friedman [4] and future fire safety requirements and research needs for space exploration are described in reference [5]. Few studies have addressed the issue of material flammability for spacecraft applications. The relevance of Test 1 to material flammability for micro-gravity applications was explored by Ohlemiller and Villa [6]. Ohlemiller and Villa conducted a series of tests following the protocol of Test 1, modify the test to include pre-heating by external radiation and compared the results with tests conducted with the cone calorimeter and the L.I.F.T. (ASTM-E-1321). This work will be described in more detail, in following sections, since it provides significant insight to the issues addressed in this work. Following the recommendations of Ohlemiller and Villa [6], Cordova et al. [7] and Long et al. [8] presented some preliminary results on the adaptation of the L.I.F.T. apparatus (ASTM-E-1321) to asses the performance of materials for micro-gravity applications. In their work they suggest the use of a forced flow version of the L.I.F.T. to determine the potential of a material to ignition and lateral (opposed) flame spread. Recent experiments conducted in the Skorost combustion tunnel apparatus on board of the Orbital Station MIR [9] have shown that there a limiting velocities below which a diffusion flame established over PMMA, Delrin and high-density polyethylene ceases to exist. Flow shutoff was therefore deemed to be an appropriate methodology to follow the detection of a fire where flames were observed to extinguish in less than twenty seconds after the suppression of the flow.

Criticism towards the use of the current methodology is common in the micro-gravity combustion literature [10] where studies have challenged the concept of co-current spread as being a worst case scenario [11-13] and even reverse flammability rankings have been presented [14]. The imminent construction of the Space Station and the projected Human Mission to Mars, due to the extent of the missions, high voltage of the on-board power supplies and greater volume of high temperature scientific instrumentation will result in enhanced hazard and more frequent fire initiation events [9]. Therefore,

there is a strong need to evaluate these protocols using fundamental combustion principles. This work has the overall objective of providing flammability criteria for micro-gravity environments beyond the considerations given in reference [1].

NOMENCLATURE

a	Absorptivity
A	Pre-exponential constant
B	Mass transfer number
B_T	Modified mass transfer number
C	Specific heat
$\overline{C}$	Co-current flame spread constant
$\overline{D}$	Damköhler number
ΔH_C	Heat of combustion
ΔH_p	Heat of pyrolysis
E	Activation energy
f	Normalized stream function
h_c	Convective heat transfer coefficient
h_r	Radiative heat transfer coefficient
h_T	Total heat transfer coefficient
k	Thermal conductivity
L	Characteristic length scale
$\dot{m}''$	Mass flux
$\dot{q}''$	Heat flux
$\dot{q}''_{0.ig}$	Critical heat flux for ignition
Q	Normalized surface total heat losses
R^0	Universal constant
Re	Reynolds number
t	Time
T	Temperature
u	Air velocity
U_∞	Characteristic air velocity
x	In-depth coordinate
x_p	Pyrolysis length
Y	Mass fraction
Z	Shvab-Zeldovich variable

Greek Symbols

α	Thermal diffusivity
β	Mixture fraction
χ	Radiative fraction
δ	Characteristic heating length
ε	Characteristic thermal penetration length
η	Self-similarity variable
ρ	Density
τ_{CH}	Characteristic chemical time
τ_r	Characteristic residence time
ψ	Stream function

Sub-indeces

∞	Infinity
C	Characteristic
C,S	Co-Current (forward) spread
e	External
f	Flame
f,c	Heat convected from the flame
f,r	Heat radiated from the flame
F	Fuel
F,L	Fuel lean limit
g	Generated
i	Induction
ig	Ignition
L	Loss
L,c	In-depth conduction
L,rf	Flame radiative heat loss
L,rs	Surface radiative heat loss
m	Mixing
O	Oxygen
O,S	Opposed (Counter-Current) spread
p	Pyrolysis
T	Total

METHODOLOGY

Proper evaluation of material flammability requires understanding of the flame structure, the degradation process of the material and the interface (boundary condition) between the two. A simple model for the ignition process based on previous studies will be used here [15-20]. When the material, initially at $T_{\infty,}$ is subject to a heat insult ($\dot{q}''_e$) the temperature rises and a temperature distribution function of the location and time is created inside the material (T(x,t)). The surface temperature ($T_S(0,t)$) will increase but the material will not release any flammable gases (Figure 1(a)) until a pyrolysis temperature is attained (T_P) (Figure 1(b)). The time necessary to achieve the pyrolysis temperature is generally referred as the time to pyrolysis, t_P. Throughout the pre-heating period the fuel concentration in the gas phase can be considered negligible. The absence of gas phase fuel does not preclude degradation of the material, generally, throughout the preheating process, the material degrades and subsequently its thermal properties change. Once the pyrolysis temperature is attained the fuel concentration increases until it attains a “lean flammability limit” ($Y_{F,L}$). The time necessary to reach this fuel concentration is called the “mixing time” or “time to attain a flammable mixture” (t_m). At this point, the temperature of the gases rises until a self-sustained exothermic reaction is attained. This period is called the “induction time” (t_i) and can be achieved by heating of the mixture (auto-ignition) or by means of a pilot or hot spot (piloted ignition). Piloted ignition is illustrated in Figure 1(c).

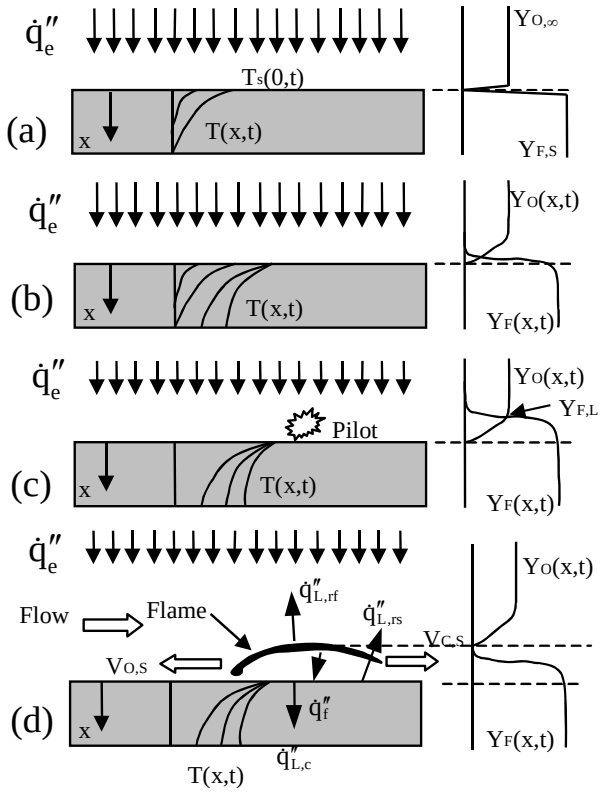

Figure 1. Schematic of the sequence of events leading to the ignition and subsequent growth of a fire established over a combustible surface.

It is important to note that after pyrolisis is initiated the net heat flux to the surface is used entirely for pyrolisis and no subsequent temperature increase is noted. At this point a flame might not establish over the surface of the fuel because the pyrolysis rate remains too small to sustain a flame, this period is characterized by flashing. The pyrolysis rate will increase with time increasing the frequency of the flashing until a flame is fully established. Once a flame is established the growth process follows. In the presence of a flow (i.e. HVAC induced flows) spread can be of two types, opposed ($V_{O,S}$) and co-current ($V_{C,S}$). Opposed flame spread goes against the flow and co-current in the direction of the flow (Figure 1(d)). The flame enhances the heat feedback to the unburned surface increasing its temperature to T_p, leading to the production of flammable gases and resulting in subsequent pilot ignitions. For spread, the existing flame can be considered the pilot. Opposed and co-current spread are complex phenomena, the former related to leading edge characteristics and the latter depending on the flame geometry and characteristics. The net heat supply to the surface ($\dot{q}''_f$) is established by the flow structure, the heat generated by the flame ($\dot{q}''_g$) and radiative losses ($\dot{q}''_{L,rf}$). A fraction of this heat is used for fuel pyrolisis ($\dot{q}''_S$) and the rest is lost to the flow, by radiation from the surface to the environment ($\dot{q}''_{L,rs}$) or through the material by conduction ($\dot{q}''_{L,c}$). Although heat supply is controlled by gas phase dynamics, the preheating process is controlled by the thermal properties of the degrading material.

Heat and mass transfer mechanisms in normal and micro-gravity differ greatly. Since natural convection induces a flow of approximately 0.5 m/s independent of the relative location of the surface with respect to the gravity vector. The result is a different flame geometry, ignition, spread and extinction characteristics. Figure 2 shows clearly the difference between a normal and micro-gravity flame. Micro-gravity flames are blue and very close to the surface, heat feedback occurs mostly at the leading edge and downstream of the flame. In normal gravity, a buoyant plume dominates the geometry of the flame and heat feedback can not be neglected in any direction since radiation contributes to pre-heating upstream of the flame. The significant differences between normal and micro-gravity flames require exploration of flammability criteria under conditions relevant to spacecraft. Normal gravity criteria will not be necessarily applicable to micro-gravity.

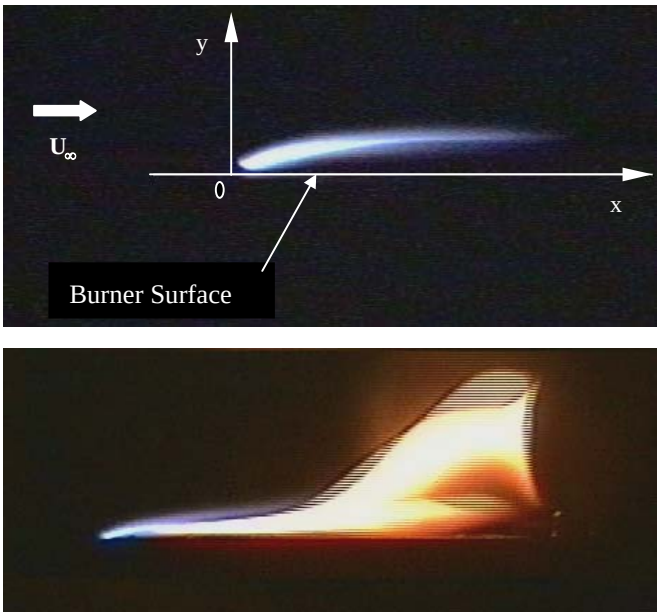

Figure 2 – Images of a micro-gravity flame (top) and a normal gravity flame (bottom). Both cases correspond to $U_\infty = 200\,\text{mm/s}$ and $Y_{O,\infty}$=0.235.

IGNITION

Based on the above model, and approximate evaluation of the ignition delay time (t_{ig}) can be done by independent evaluation of all three characteristic times and their subsequent addition

$$t_{ig} = t_p + t_m + t_i \qquad (1)$$

Under fast chemical kinetic conditions (low gas velocities and elevated oxygen concentrations), introducing a strong pilot reduces the induction time (t_i) making it negligible when compared to t_p and t_m. Also, the period where the transient evolution of the fuel concentration in the gas phase increases towards a flammable mixture (t_m) has been commonly considered short when compared to heating of the solid fuel sample. Therefore, the fuel and oxidizer mixture has been normally considered to become flammable almost immediately after pyrolysis starts. Figure 3 provides data obtained using black PMMA as fuel that, although shows some discrepancy, especially for $\dot{q}''_e < 20 \ \ kW/m^2$, serves to justify this assumption. Pyrolysis temperatures and times are thus commonly referred to as ignition temperature (T_{ig}) and ignition delay time (t_{ig}) respectively [15,16], and equation (1) simplifies to $t_{ig} = t_p$, and T_{ig} can be defined as T_p.

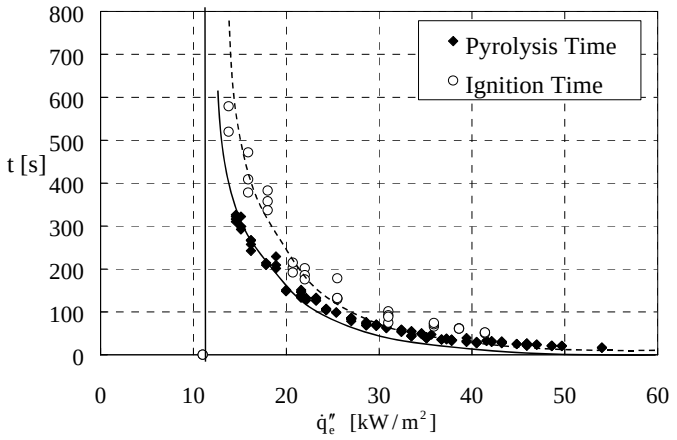

Figure 3 Ignition (t_{ig}) and pyrolysis (t_p) delay times for black PMMA in normal gravity. Tests were conducted using the LIFT (ASTM-1321) and the pyrolysis time was defined as the first observed gases emerging from the surface and visualized by means of a Laser sheet.

Under these assumptions the solid heating process is described by the energy equation:

$$\frac{\partial^2 T}{\partial x^2} = \frac{1}{\alpha}\frac{\partial T}{\partial t} \qquad \begin{array}{ll} \text{B.C.} & \\ x=0, & -k\frac{\partial T}{\partial x} = \dot{q}''_S(0,t) \\ t = 0 & \\ x \to \infty & T = T_\infty \end{array} \tag{2}$$

The classical analysis [14] assumes a linear approximation for the surface re-radiation. Thus, assuming that the total heat transfer coefficient (h_T) is equal to the sum of the convective heat transfer coefficient (h_c) and the radiative heat transfer coefficient (h_r), the following expression defines the net heat flux ($\dot{q}''_s$) at the surface of the solid fuel.

$$\dot{q}''_S(0,t) = a\dot{q}''_e - h_T(T(0,t) - T_\infty) \tag{3}$$

By non-dimensionalizing all variables in the following way

$$\bar{T} = \frac{T - T_\infty}{T_{ig} - T_\infty}$$

$$\bar{x} = \frac{x}{x_c} \text{ where } x_c = k/h_T$$

$$\bar{t} = \frac{t}{t_c} \text{ where } t_c = k\rho C/{h_T}^2 \text{ and}$$

$$\dot{\bar{q}}'' = \frac{\dot{q}''}{\dot{q}''_c} \text{ where } \dot{q}''_c = h_T(T_{ig} - T_\infty)/a$$

the following solution is obtained for the evolution of the temperature in the sample

$$\bar{T}_S = \dot{\bar{q}}''_e\left[1 - e^{\bar{t}}\,\mathrm{erfc}(\sqrt{\bar{t}}\,)\right] \tag{4}$$

To solve for the ignition time ($\bar{t}_{ig}$) a first order Taylor series expansion of equation (4) is conducted. The range of validity of this expansion is limited, thus can not be used over a large range of incident heat fluxes. Consequently, the domain has to be divided at least in two. The first domain corresponds to high incident heat fluxes where the ignition temperature ($\bar{T}_{ig}$) is attained very fast, $\bar{t}_{ig} \to 0$. Application of the first order Taylor Series Expansion yields:

$$\bar{t}_{ig} = \frac{\pi}{4}\frac{1}{(\dot{\bar{q}}''_e)^2} \tag{5}$$

The second domain corresponds to incident heat fluxes close to the critical heat flux for ignition ($\dot{\bar{q}}''_{0,ig} \approx 1$) where the ignition temperature ($\bar{T}_{ig}$) is attained very slow, $\bar{t}_{ig} \to \infty$.

$$\bar{t}_{ig} = \frac{1}{\pi}\left(\frac{1}{1 - 1/\dot{\bar{q}}''_e}\right)^2 \tag{6}$$

At $\dot{\bar{q}}''_{0,ig} \approx 1$ the surface will attain the ignition temperature ($\bar{T}_{ig}$) at equilibrium, therefore if $\dot{\bar{q}}''_e < \dot{\bar{q}}''_{0,ig} \approx 1$ the surface will never reach the pyrolysis temperature.

The use of a linearized total heat transfer coefficient has been questioned in the literature [17] and corrections that incorporate the non-linear nature of surface re-radiation have been proposed [18]. Temperature histories for different external heat fluxes are presented in Figure 4. By fitting the theory to the temperature histories a global heat transfer coefficient can be obtained and it can be seen that excellent agreement is found between theory and experiments for a wide range of external heat fluxes ($\dot{\bar{q}}''_e \approx 1.1$ to $\dot{\bar{q}}''_e \approx 4$). For $\dot{\bar{q}}''_e \approx 4$ and average temperature history is presented but for $\dot{\bar{q}}''_e \approx 1.1$ individual recordings are shown.

The individual recordings serve to show the difficulty of acquiring temperature measurements with thermocouples. At a

certain point the thermocouples will separate from the surface, this can occur in a random manner (as shown by Figure 4). While the thermocouple is attached to the surface the temperature follows well theory. The material properties used for PMMA are provided in table 1 and where obtained from different sources listed by Hallman [21] and Steinhaus [22].

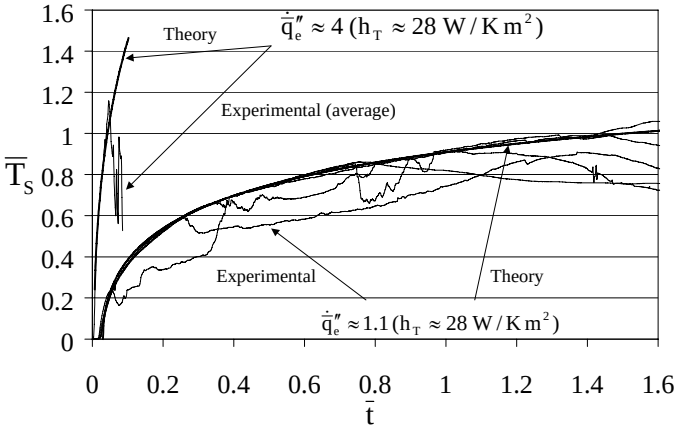

Figure 4 Evolution of the surface temperature ($\overline{T}_S$) with time ($\bar{t}$), comparison between the theoretical predictions and the experimental values. For $\dot{\bar{q}}''_e \approx 4$, an average experimental value of 32 thermocouple histories (thin line) is compared with the theoretical prediction calculated with $h_T \approx 28\ W/K\,m^2$ (thick line). For $\dot{\bar{q}}''_e \approx 1.1$, individual thermocouple histories (thin lines) are compared with the theoretical prediction calculated with $h_T \approx 28\ W/K\,m^2$ (thick line).

Property	
C [J/kg.K]	2,020
ρ [kg/m^3]	1,180
k [W/m.K]	0.192
a	0.85
T_{ig} [K]	538
T_∞[K]	293
h_T [W/m^{2}K]	28

Table 1 Thermal properties of black Poly(Methylmethacrylate) as compiled by Hallman [21] and Steinhaus [22]. All properties are evaluated at an average temperature of 373 K.

For most materials currently used in construction, furnishings and specially those used in aerospace applications, evaluation of the thermal properties of the material is not possible. Therefore the above analysis is fit to experimental evaluation of the ignition delay time (equations (5) and (6)) and the thermal inertia "kρC" and T_{ig} can be evaluated.

The value of h_T is determined by fitting the solution to temperature histories and T_{ig} is extracted from the critical heat flux for ignition, $\dot{q}''_c = \dot{\bar{q}}''_{0,ig} = h_T(T_{ig} - T_\infty)/a$. The emissivity of the material is introduced whenever it can be determined but generally it is assumed to be unity since the materials tend to blacken when exposed to the external heat flux [14]. A series of reference materials together with some typical of spacecraft applications have been tested following conventional protocols [7,8,15,16]. The data non-dimensionalized per equations (5) and (6) is presented in Figure 5. Table 2 presents the list of materials used and the properties used when correlating the data.

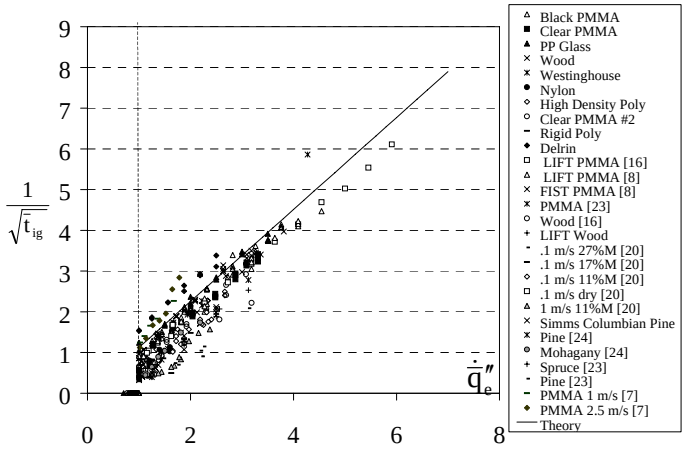

Figure 5 Evolution of the ignition delay time with the external heat flux. Comparison of experimental data of the present study with the theoretical predictions and data from the literature.

CONSIDERATIONS PERTAINING MICRO-GRAVITY

When ignition is conducted under conditions typical of spacecraft convective heat and mass transfer is modified due to the absence of buoyancy and the weak forced flow. Equation (1) can no longer be simplified to $t_{ig} \approx t_p$ and the effect of a net reduction of convective transport needs to be evaluated. The convective heat transfer coefficient is reduced from approximately 20 kW/m^{2}K to 2 kW/m^{2}K leading to a reduction in t_p and $\dot{q}''_c$. The reduction of h_T will have a decreasing effect on the total ignition delay time as the external heat flux increases and can be incorporated in the theoretical development that leads to equation (5). The data corresponding to micro-gravity conditions could be included in Figure 5. Experimental data for micro-gravity conditions is difficult to obtain, since the characteristic ignition delay times are longer than the experimental time provided by ground based micro-gravity facilities (t<30 s.) thus data points can be obtained only for very high heat fluxes ($\dot{q}''_e > 25\ kW/m^2$). At this high heat fluxes the ignition delay time is represented by equation (5),

thus is independent of the convective heat transfer coefficient. Theory predicts that the ignition delay time should be very similar in normal and micro-gravity. Experimental results reported by Roslon et al [25] show that for PMMA and a polypropylene/glass composite the ignition delay time decreases significantly (up to 50% in the some cases). The significant variation of the ignition delay time can be attributed to the combined effect of varying the time to attain pyrolysis and the mixing time. Under the assumption that ignition will occur when a flammable mixture is attained (lean flammability limit), a reduction in convective transport implies a reduction in t_m. Therefore the mixing time (t_m) needs to be analyzed and, in the presence of a strong pilot, equation (1) can be only reduced to $t_{ig} \approx t_p + t_m$.

Material	$k\rho C$ $(kW/m^2K)^2s$	$\dot{\bar{q}}''_{0,ig}$ (kW/m^2)
LIFT Wood [16]	0.29	16
LIFT Wood	0.17	16
FIST Wood [8]	0.14	16
LIFT black PMMA [16]	2.08	9
LIFT black PMMA	1.40	11
FIST black PMMA [8]	1.24	11
Clear PMMA	0.58	12.5
Delrin	0.59	16
High Density Polyethylene	0.46	15
Nylon	0.13	25
Rigid Polyethylene	0.12	24
PP/Glass Composite	0.91	10
Clear PMMA #2	0.56	13
Westinghouse Glass/Epoxy Laminate	0.52	18

Table 2 Material properties from ignition tests as obtained from the ignition delay times.

It was shown by Long et al. [8] that, under normal gravity conditions, the fuel mass fraction could be obtained by means of an integral analysis of the boundary layer formed upstream of the pilot. Thus the fuel mass fraction at the pilot (Y_F)can be defined as:

$$Y_F = \frac{\dot{m}'_F}{\dot{m}'_F + \dot{m}'_O} \tag{7}$$

Where $\dot{m}'_F$ and $\dot{m}'_O$ are the mass flux of fuel and oxidizer respectively, integrated over the stream wise coordinate. Long et al. [8] proposed a model to determine Y_F and showed that ignition occurred at a constant value of the fuel mass fraction that they labeled the lean flammability limit, Y_{FL}. This interpretation could serve to predict the ignition delay time in micro-gravity but the uncertainty in the flow structure during the parabolic flight experiments reported by Roslon et al. [25] make this comparison difficult at this point. Long-term micro-gravity experiments will allow a better validation of theory with experimental results.

COUNTER-CURRENT (OPPOSED) FLAME SPREAD

Opposed flame spread can be described in a simple manner by assuming that all the heat from the flame ($\dot{q}''_f$) plus any external heat flux ($\dot{q}''_e$) is used to compensate for heat losses from the surface ($\dot{q}''_L$) and to heat the material from its ambient temperature to the ignition temperature. The volume heated is determined by two characteristic length scales, $\delta_{O,S}$ in the direction of propagation and $\varepsilon_{O,S}$ in the direction perpendicular to the surface. The following expression serves to describe conservation of energy:

$$\delta_{O,S}(a\dot{q}''_S) = \varepsilon_{O,S} V_{O,s}\left[\rho C(T_{ig} - T_\infty)\right] \tag{8}$$

where the net heat flux at the surface is given by

$\dot{q}''_S = \dot{q}''_f + \dot{q}''_e - \dot{q}''_L$

and the losses can again be defined as a function of the linearized heat transfer coefficient

$$\dot{q}''_L = \frac{h_T(T_S - T_\infty)}{a}$$

The boundary condition at the surface eliminates the characteristic penetration depth, ε, from equation (8). Non-dimensionalizing all variables using the same characteristic values as defined in the ignition section and defining a characteristic propagation velocity

$$V_C = \frac{x_C}{t_C}$$

a non-dimensional spread velocity can be obtained

$$\overline{V}_{O,S} = \frac{V_{O,S}}{V_C} = \overline{\delta}_{O,S}(\dot{\bar{q}}''_S)^2 = \phi_{O,S} \tag{9}$$

Where the term $\phi_{O,S}$ is a global parameter that includes the heat flux from the flame and the characteristic length scale of the pre-heating that generally depend on many parameters (oxygen concentration, flow velocity, fuel, etc.) and is very difficult to evaluate.

A useful way of obtaining a good estimate of $\phi_{O,S}$ is by exposing the sample to a prescribed external heat flux and allowing the sample to reach thermal equilibrium before initiating propagation. Equation (9) can be re-written to

$$\overline{V}_{O,S} = \left[\frac{\dot{\bar{q}}''_f}{(1-\dot{\bar{q}}''_e)} - 1\right]^2 \overline{\delta}_{O,S} \tag{10}$$

Under conditions corresponding to the LIFT test (normal gravity, lateral propagation) $\dot{\bar{q}}''_f >> \dot{\bar{q}}''_e$ therefore

$$\frac{\dot{\bar{q}}''_f}{(1-\dot{\bar{q}}''_e)} >> 1 \qquad (11)$$

So equation (9) can be re-written as

$$\overline{V}_{O,S} = \frac{\phi_{O,S}}{(1-\dot{\bar{q}}''_e)^2} \qquad (12)$$

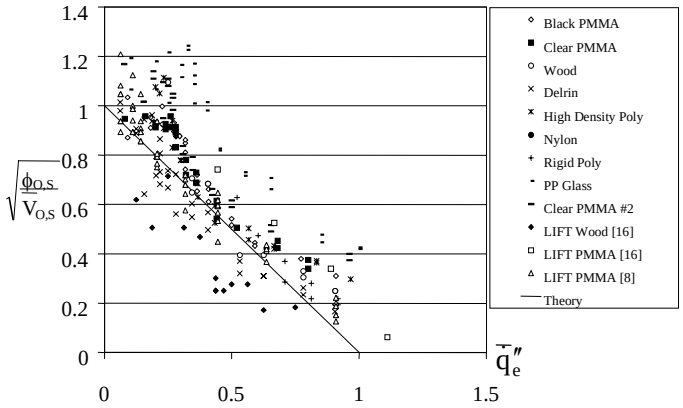

Figure 6 Evolution of the opposed flame spread velocity with the external heat flux. Comparison of experimental data of the present study with the theoretical predictions and data from the literature. Not shown is the data for Nylon since it went beyond the scale. Nylon melted showing thus was inappropriate for the present testing protocol.

Where the term $[(\dot{\bar{q}}''_f)^2 \overline{\delta}_{O,S}]$ becomes $\phi_{O,S}$. The experimental data scaled by means of the characteristic values is presented in Figure 6. The dimensional value of $\phi_{O,S}$ (following the LIFT (**L**ateral **I**gnition and **F**lame spread **T**est) methodology [16]) can be obtained by conducting experiments at different external heat fluxes is presented in Table 3. It has to be noted that due to their particular mechanical properties, some materials can not be described by the proposed methodology. From the materials studied Nylon showed a random behavior leading to spread velocities, that once scaled, appeared off the scale on Figure 6. This is a limitation that is applicable to any testing methodology and in this case the materials that show a differing need to be evaluated on an individual basis independent of any standard methodology.

CONSIDERATIONS PERTAINING MICRO-GRAVITY

If opposed flame spread can be considered a series of consecutive piloted ignitions, the same considerations presented for the ignition delay time will be appropriate for opposed flame spread. The reduced convective heat transfer coefficient will lead to a different equilibrium temperature but equation (10) will remain valid. In normal gravity and away from extinction conditions, $\dot{\bar{q}}''_f >> \dot{\bar{q}}''_e$ therefore equation (10) could be simplified leading to equation (12) and a constant value of $\phi_{O,S}$ can be obtained experimentally. In micro-gravity reduced transport of oxygen to the flame results in an increase in importance of radiative heat losses from the flame to the environment that lead to a reduction of the spread rate and eventually to extinction [9-14]. For this particular methodology, this will translate to a variation of the value of $\phi_{O,S}$. Predictions of how this value will change as the external heat flux is reduced and the flame approaches extinction is not trivial since the flame contribution and characteristic preheating length scale will both change. No experimental data is available at this point to validate this approach but equation (10) shows that $\phi_{O,S}$ and $\overline{\delta}_{O,S}$ are the non-dimensional parameters controlling opposed flame propagation.

Material	$\phi_{O,S} * (x_C \dot{q}''_{0,ig} / V_C)$ (kW^2/m^3s)
LIFT Wood [16]	0.04
FIST Wood [8]	0.04
LIFT black PMMA [16]	0.01
LIFT black PMMA	0.01
FIST black PMMA [8]	0.01
Clear PMMA	0.01
Delrin	0.02
High Density Polyetylene	0.01
Nylon	0.32
Rigid Polyetylene	0.02
PP/Glass Composite	0.01
Clear PMMA #2	0.01
Westinghouse Glass/Epoxy Laminate	No Spread

Table 3 Flame spread properties obtained following the LIFT methodology [16] for different common materials and materials relevant to spacecraft.

CO-CURRENT (FORWARD) FLAME SPREAD

Co-current flame spread can be described using the same simplified methodology as opposed flame spread. Where conservation of energy will give an expression similar to equation (7) which is presented by equation (14)

$$\delta_{C,S}(a\dot{q}''_S) = \varepsilon_{C,S} V_{C,s} \left[\rho C (T_{ig} - T_\infty)\right] \qquad (13)$$

where the net heat flux at the surface is given by

$$\dot{q}''_S = \dot{q}''_f + \dot{q}''_e - \dot{q}''_L$$

and the losses can be defined as the convective contribution of the flame and a linearized surface re-radiation. Radiation absorption by the flame is neglected.

$$\dot{q}''_L = \frac{h_C(T_{ig} - T_F)}{a} + \frac{h_r(T_{ig} - T_\infty)}{a}$$

Scaling equation (13) in a similar manner as for opposed flame spread leads to the following expression

$$\overline{V}_{C,S} = \frac{V_{C,S}}{V_C} = \overline{\delta}_{C,S}(\dot{\overline{q}}''_S)^2 = \phi_{C,S} \qquad (14)$$

For this mode of spread the characteristic length scale is generally referred as the flame length and is given by

$$\overline{\delta}_{C,S} = \frac{L_f - x_P}{x_C}$$

Where L_f is the distance from the leading to the trailing edge of the flame and x_P is the length of the pyrolysis region.

In the same manner as for opposed flame spread the surface can be exposed to external radiation ($\dot{q}''_e$) until the surface reaches thermal equilibrium (T_S) before ignition of the flame. Equation (14) can be re-written to

$$\overline{V}_{C,S} = \frac{\phi_{C,S}}{[1 - \dot{\overline{q}}''_e]^2} \qquad (15)$$

Where $\phi_{C,S}$ can be evaluated in a similar manner to $\phi_{O,S}$. The definition of $\phi_{C,S} \approx [(\dot{\overline{q}}''_S)^2 \overline{\delta}_{C,S}]$ needs further exploration since $\dot{\overline{q}}''_S$ includes a flame radiation component ($\dot{\overline{q}}''_{f,r}$) the convective heat flux from the flame ($\dot{\overline{q}}''_{f,c}$) and surface re-radiation ($\dot{q}''_{L,rs} = \dot{\overline{q}}''_{0,ig} \approx 1$). Therefore, the net heat flux to the surface is given by

$$\dot{\overline{q}}''_S = \dot{\overline{q}}''_{f,r} + \dot{\overline{q}}''_{f,c} - 1$$

Micro-gravity flames are subject only to the low flow velocities imposed by the heating, ventilation and air conditioning units (HVAC), therefore the characteristic velocity is approximately 0.1 m/s and thus the flames are expected to be laminar. Under these conditions it was shown by Orloff et al [26] that all three components of the net heat flux to the surface are of comparable magnitude and the convective mode is the only form of heat transfer that increases as the flow decreases (Figure 7). It was later shown by Pagni and Shih [27] that $\dot{\overline{q}}''_{f,r} \approx 1$ thus canceling out with surface re-radiation and leaving only the convective component as the net heat flux to the surface. Convective heat transfer to the surface can be studied by assuming that the gas phase is much faster than the solid phase and propagation can be treated as a series of quasi-steady solutions to a reactive boundary layer [28]. The heat flux to the surface can be obtained as a function of the mass transfer number ("B" number) which is a property of the material. Further analysis shows that the flame length is also a function only of the "B" number [26] which leads to the conclusion that $\phi_{C,S}$ is a function only of the mass transfer number, and thus a material property.

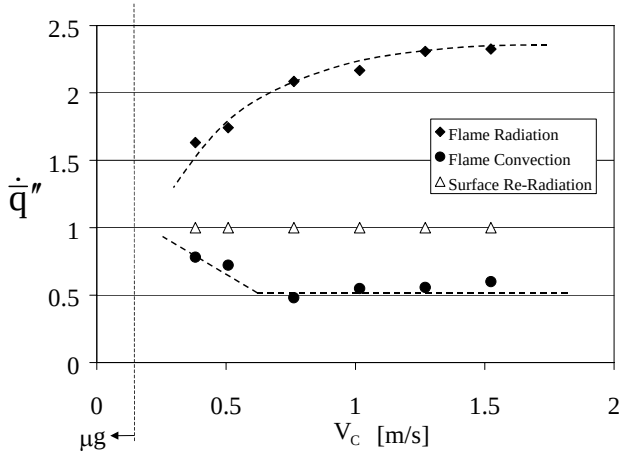

Figure 7 Comparison of the magnitude of the different modes of heat transfer. The data was extracted from the experiments conducted by Orloff et al [26].

Based on these premises it can be assumed that

$$\overline{\delta}_{C,S} \approx \overline{C}\,\overline{x}_P \qquad (16)$$

Where "$\overline{C}$" is a constant function of the mass transfer number. The value of "$\overline{C}$" can be obtained from the solution proposed by Pagni and Shih [27] but this solution assumes infinite chemistry and therefore, tends to over-predict the experimental values. Experimental data has been correlated and the correlation proposed by Orloff et al. [26] is presented in Figure 8. As it can be seen in Figure 8, once the characteristic velocity exceeds a specific value (V_C>1500 mm/s) the flow becomes turbulent and flame radiation affects the characteristic length, and the experimental data can be correlated by $\overline{\delta}_C \approx 0.625\,(\overline{x}_P)^{0.781}$. Different correlations have been proposed for the turbulent regime, these are summarized in reference [29] but will not be discussed here since the laminar regime is the one of interest in micro-gravity.

For normal gravity experiments the above formulation seems to describe well the experimental data, $\dot{\overline{q}}''_S \approx \dot{\overline{q}}''_{f,c}$ and the characteristic length scale becomes a function only of the mass transfer number. Equation (15) is valid and therefore $\phi_{C,S}$ becomes a function only of x_P and the thermal properties of the fuel and oxidizer. These simplifications allow to solve equation (14) to obtain the co-current flame spread velocity, $\overline{V}_{C,S}$. Such expressions are abundant in the literature and have been summarized by Fernandez-Pello [29].

For micro-gravity, Figure 8 shows that the simplifications that lead to equation (16) are no longer valid and $\overline{\delta}_{C,S} / \overline{x}_P$ is not a constant. There is no data available in the literature to describe the transitional regime between 500 mm/s $<V_C<$ 1,000 mm/s. It is, therefore, not clear where these assumptions break down, but extrapolation of the trends shows that the intercept will occur around 900 mm/s or a pyrolysis length of approximately 50 mm. The following sections will provide an analysis of the assumptions that are the basis of the above analysis and an evaluation to their relevance for micro-gravity conditions will be presented.

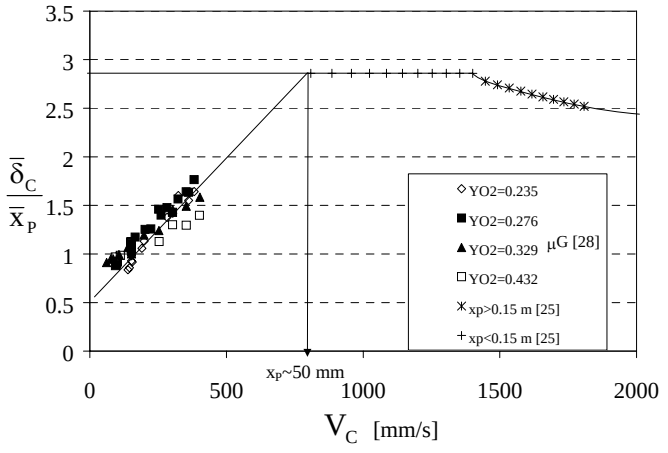

Figure 8 Characteristic length scale ($\overline{\delta}_{C,S}$) normalized by the pyrolysis length ($\overline{x}_P$). The data presented includes the correlations obtained in reference [26] and micro-gravity data presented in reference [28]. The normal gravity data corresponds to upward flame spread experiments and was originally presented as a function of a dimensional $\overline{x}_P$, the conversion to velocity was done to compare normal-micro-gravity data and was achieved by deriving a characteristic velocity induced by buoyancy as done in reference [27].

THE FLAME

A detailed analysis of the phenomena occurring downstream of the flame leading edge is necessary to extract the mechanisms controlling co-current flame spread. This analysis is based on the pioneering study of Emmons [30].

The classical Shvab-Zeldovich approach proposed by Emmons [30] can be easily found in the literature so only a brief summary will be presented here. By making boundary layer type assumptions the flow can be described by

$$f''' + f \cdot f'' = 0 \qquad (17)$$

Where $f = \frac{\psi}{(x/Re)^{1/2}}$ and ψ is the stream function, x the stream coordinate and Re the Reynolds number. Equation (17) is coupled to a single ordinary differential equation that incorporates conservation of energy and species

$$\beta'' + f \cdot \beta' = 0 \qquad (18)$$

Where β is the mixture fraction and is given by $\beta = \frac{Z_i - Z_{i,0}}{Z_{i,\infty} - Z_{i,0}}$ and Z_i are the traditional Shvab-Zeldovich variables. The boundary conditions are:

$$\eta = 0 \quad , \quad f' = 0 \quad , \quad \frac{f}{f''} = -\frac{B}{2} \quad , \quad \beta = 0$$
$$\eta \to \infty \quad , \quad f' = 2 \quad , \quad \beta = 1$$

where $\eta = \frac{1}{2}\left(\frac{Re}{x}\right)^{1/2} \int_0^y \rho dy$ is the self-similar variable and

$$B = \frac{\Delta H_C Y_{O,\infty} - C(T_S - T_\infty)}{\Delta H_P + Q} \qquad (19)$$

is the mass transfer number. The right hand term corresponds to the energy necessary to bring the gas from T_∞ to T_S. The heat of pyrolysis is denoted by ΔH_P and Q represents other losses at the fuel surface per unit mass of fuel produced

$$Q = \dot{q}''_L / \dot{m}''_f \qquad (20)$$

The fuel mass flux at the surface results from the self-similar solution

$$\dot{m}''_f = (\rho_\infty U_\infty) \frac{(\eta f' - f)}{2(Re.(x/L))^{1/2}} \qquad (21)$$

The above approach requires radiative heat transfer from the flame to the surface and to the environment to be neglected and re-radiation from the surface and in-depth absorption and conduction are only implicitly incorporated through the term Q. The Boundary layer flow needs to be preserved therefore can not be used to describe the leading edge or if the flow is significantly perturbed by the flame. Emmons [30] noted that if heat flux to the surface exceeded a "blow-off" limit separation of the flow will occur and heat transfer to the flame will be blocked and extinction will follow. Pagni and Shih [27] added that radiative feedback from the flame to the surface could lead to this condition.

Attempts to correct for these limitations can be found in the literature. Pagni and Shih [27] neglected Q and defined an adiabatic mass transfer number, B_A (i.e.for PMMA and air, B_A =3.3). By incorporating a corrective factor, R, radiative exchange from the flame to the environment was incorporated and the mass transfer number was re-defined as $B = R\, B_A$. It was noted that surface re-radiation and radiative feedback from the flame are of similar magnitude and therefore could be neglected. Estimation of the radiative feedback and surface re-radiation shows that the flame temperature and the presence of soot affect this balance. For low Reynolds number flames this balance has been shown to be negative and leading to quenching of the flame [31-33] therefore surface re-radiation, radiative heat feedback to the surface and radiative losses from the flame to the environment have to be incorporated in "B".

Surface re-radiation and radiative feedback to the surface can be incorporated through Q and radiative losses from the flame to the environment by a factor multiplying the energy released from combustion.

If the fuel is not thermally thin, in-depth conduction and radiation absorption need to be incorporated into the "B" number and this can be done through Q. This is only possible if the gas phase can be considered to evolve much faster than the solid phase. The validity of this assumption was demonstrated by Yang and T'ien [33] for similar dimensions and flow conditions, therefore will not be repeated here.

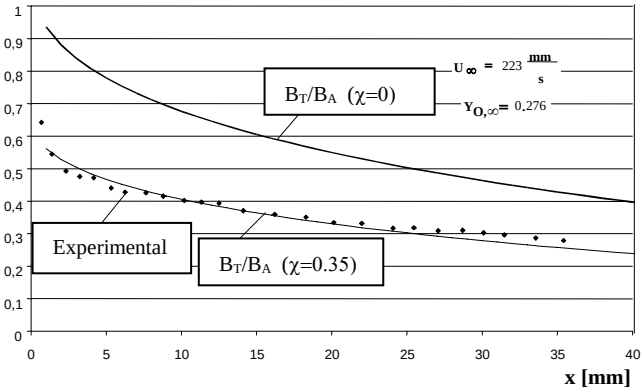

Figure 9 Variation of B_T / B_A as a function of the streamwise coordinate, x. The experimental data used to determine the value of χ ($\chi \approx 0.35$) was extracted from Vietoris et al. [28].

Introducing all the above heat losses the "B_T" number can be redefined as

$$B_T = \frac{(1-\chi)(\Delta H_C Y_{O_2,\infty}) - Cp_\infty (T_W - T_\infty)}{\Delta H_P + Q} \qquad (22)$$

Where χ corresponds to the fraction of the total energy released by the flame that is radiated to the environment and is a function only of the emissivity of the flame.

$$Q = \frac{\left(\dot{q}''_{L,C} + \dot{q}''_{L,sr} - \dot{q}''_{fr}\right)}{\dot{m}''_f} \qquad (23)$$

Q is a function of the flame temperature (radiative losses from the flame) and the stream wise co-ordinate ("x", through $\dot{m}''_f$).

It is extremely important to note that for specific experimental conditions ($U_\infty, Y_{O,\infty}$) the importance of Q increases with the distance from the leading edge since $\dot{m}''_f$ decreases with "x" (equation (21)). This is not the case with χ that depends only on the emissivity therefore its value will be fixed by the experimental conditions. If $\chi = 0$, close to the leading edge Q approaches zero and "B_T" converges towards "B_A," as the distance from the leading edge increases B_T decreases due to the greater relative importance of heat losses to fuel mass production. Figure 9 shows the evolution of the ratio (B_T / B_A) as a function of the distance from the leading edge. The top curve shows the value for B_T / B_A for $\chi = 0$, this is done because the radiative fraction, χ, is not easy to determine. By matching the flame stand-off distance obtained from theory, using the definition of B_T proposed in equation (22), and the experimental values reported by Vietoris et al. [35], the radiative fraction can be determined. Figure 9 shows that for PMMA and air $\chi \approx 0.35$ which corresponds well with other values reported in the literature. In micro-gravity the value of χ was found to increase with the forced flow and with the oxygen concentration [35].

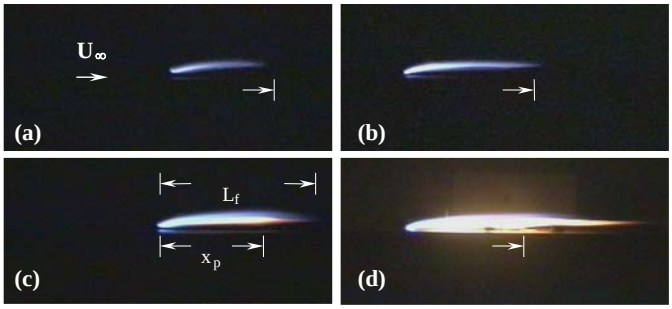

Figure 10 Characteristic images of the flames under different flow conditions (L_F is the flame length and x_p the length of the pyrolyzing fuel. (a) u_∞ = 80 mm/s (b) u_∞ = 150 mm/s, (c) U_∞ =220 mm/s, (d) U_∞ = 340 mm/s

This analysis supposes infinite chemistry and thus, flame geometry and length are determined based on thermal considerations. The flame length as derived by Pagni and Shih [27] leads to significantly larger values than those observed experimentally. Pagni and Shih [27] use B_A for their flame length calculations but even when using B_T, the flame length remains over predicted. Figure 10 shows a series of images showing the evolution of the flame length with different forced flow velocities. The figure shows the effect of the flow on the visible flame radiation (χ increases with the velocity) and that the flame length can be smaller than the pyrolysis length.

Figure 11 shows the normalized evolution of the flame length with the flow velocity. The lines show the theoretical predictions and the data the experimental values. The experimental data corresponds to that presented in Figure 8. It is clear that the infinite chemistry assumption does not allow determination of the evolution of the flame length as the flame propagates, thus is not sufficient to determine the rate of co-current spread. An analysis that explains trailing edge extinction is necessary.

Gas phase extinction is generally described by means of the Damköhler number. Following the methodology of Yang and T'ien [33] and Chen and T'ien [34] a characteristic

residence time for a flame established inside a boundary layer can be defined as

$$\tau_r = \frac{\alpha_\infty}{U_\infty^{\,2}}$$

and a characteristic chemical time

$$\tau_{ch} = \frac{1}{\rho A T \exp(-E/R^{o}T)}$$

which leads to the following definition for the Damköhler number

$$\overline{D} = \frac{\tau_r}{\tau_{ch}} = \frac{\rho_\infty A T_f \exp(-E/R^{o}T_f)}{(U_\infty^{\,2}/\alpha_\infty)} \qquad (24)$$

where T_f is the flame temperature, α_∞ is the free stream thermal diffusivity, A the pre-exponential factor, E the activation energy and R the universal gas constant.

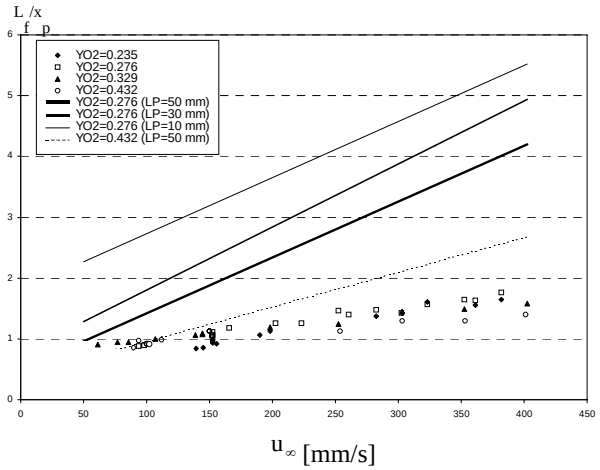

Figure 11 Normalized evolution of the flame length with the flow velocity for PMMA. The lines show the theoretical predictions and the data the experimental values.

From the solution of equation (18) it can be demonstrated that the flame temperature is almost a linear function of the mass transfer number [35]. Therefore, close to the leading edge, where heat losses to the surface are negligible and B_T is a weak function of "x", T_f, and thus the numerator, remains constant and the Damköhler number is controlled only by U_∞. The Damköhler number decreases as the forced flow velocity increases and therefore extinction close to the leading edge will occur due to an increase in U_∞ or "blow-off."

For a defined set of experimental conditions, away from the leading edge, B_T decreases in the stream-wise direction because Q increases with "x" (equations (20) and (22)). Consequently, the flame temperature will follow the same trend and the Damköhler number will decreases with "x" (equation (24)). Thus, extinction will occur at the trailing edge. As shown by equation (20), a decrease in U_∞ will result in a decrease in $\dot{m}_f''$ which in turn will increase Q (equation (22)). A relative increase of the losses leads to a decrease in B_T and consequently to a lower flame temperatures. A reduction of U_∞ has as consequence a strong reduction of the Damköhler number. This region is representative of the quenching regime where extinction will follow a decrease in U_∞.

Evaluation of the Damköhler number for PMMA is presented in Figure 12. As predicted Figure 12 shows that close to the leading edge the Damköhler number decreases with the flow velocity. Towards the trailing edge the effect of the flow velocity is reversed and thus a critical tailing edge Damköhler number can be obtained by experimentally determining the distance from the leading edge where flame quenching occurs. This critical Damköhler number is of great importance since it allows prediction of the flame length which is necessary for the evaluation of co-current flame spread.

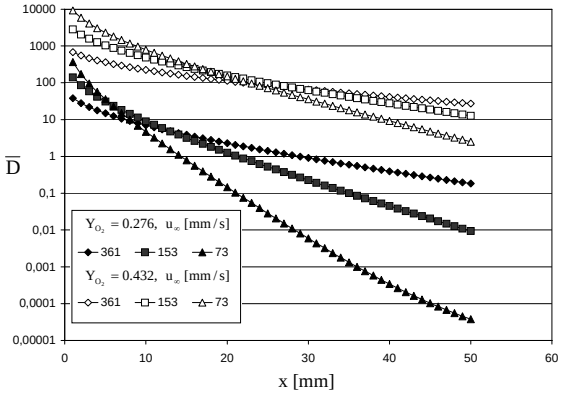

Figure 12 Evaluation of the Damköhler number as a function of the stream wise coordinate, x, for PMMA.

The concept of a critical Damköhler and corrected mass transfer "B_T" numbers can be used to provide quantitative flammability criteria for different materials but, proper evaluation of all this terms requires a detailed numerical solution as those used by West et al [36] and Yang and T'ien [33]. The uncertainties in the measurements obtained throughout the present experiments do not allow for such detail comparison. Therefore, this presentation is only done to provide a phenomenological explanation to the experimental observations. Furthermore, as the flame approaches extinction, complex gas and solid phase chemistry have to be included to fully describe the extinction process and the quasi-stationary nature of the process might be no longer valid.

CONCLUSIONS

A comprehensive methodology to assess material flammability for micro-gravity environments that addresses ignition, opposed and co-current spread has been presented as a complement to the existing methodology. Different non-

dimensional parameters have been established to rank materials and the limitations of the methodology has been established. In normal gravity $T_p \approx T_{ig}$, therefore piloted ignition can be adequately scaled by means of a characteristic temperature ($T_C = T_{ig} - T_\infty$), a characteristic length scale ($x_C = k / h_T$), a characteristic time ($t_C = k\rho C / h_T{}^2$) and a critical heat flux ($\dot{q}''_C = \dot{q}''_{0,ig} = h_T (T_{ig} - T_\infty) / a$). In micro-gravity a reduction of the convective heat transfer coefficient results in broader differences between T_p and T_{ig}. In the above scaling parameters T_{ig} needs to be replaced by T_p and the transition between the onset of pyrolysis and ignition is described by means of a lean flammability limit. Opposed flame spread is also controlled by the critical heat flux together with a parameter that describes the flame heat contribution to propagation ($\phi_{O,S}$). In normal gravity $\phi_{O,S}$ is a constant value and can be considered a material property. In micro-gravity, as the characteristic velocity decreases and $(\dot{\bar{q}}''_f / (1 - \dot{\bar{q}}''_e)) \approx 1$, radiative heat losses from the flame will affect the magnitude of $\phi_{O,S}$. Co-current flame spread in a laminar flow can be described by means of the same parameters ($\phi_{C,S}$ and $\dot{q}''_{0,ig}$) under the assumption that the $\dot{\bar{q}}''_{f,r} \approx 1$. In micro-gravity this assumption breaks down and the relevant property that controls the flame geometry and co-current spread are a modified mass transfer number, B_T. Quenching at the trailing edge is established through a minimum value of BT or a critical Damköhler number ($\overline{D}$). Different experimental results have shown the potential of this methodology in providing scientific criteria for material flammability for micro-gravity applications but complete validation is still necessary.

ACKNOWLEDGMENTS

The work related to the LIFT was funded by NASA Glenn under grant NAG-31961. The authors wish to thank Prof. A.C. Fernandez-Pello and co-workers at the University of California, Bekeley for their extensive contributions to this part of the work. Technical discussions and support of Prof. J.G. Quintiere (University of Maryland) and Dr. Howard Ross (NASA Glenn) have been crucial in the development of this study. The work on the gas phase, solid phase and Mini-Texus 6 was funded by ESA and CNES. The support of Drs. O. Minster and W. Herfs has been invaluable. JLT was partially funded by the Minta Martin Research Foundation at the University of Maryland. The contributions of the many graduate students involved in these projects at UMD, UCB and LCD have made them possible.

REFERENCES

1. "Flammability, Odor, Offgassing, and Compatibility Requirements and Test Procedures for Materials in Environments that Support Combustion" NASA-NHB 8060.1, 1981.
2. "Materials Selection List for Space Hardware Systems" MSFC-HDBK-527-REV F, September 30, 1988.
3. "Heat Release in Fires," Babrauskas, V. and Grayson, S.J. Editors, Elsevier Applied Science, 1992.
4. Friedman, R. "Fire Safety Practices in the Shuttle and the Space Station Freedom," *Second International Micro-gravity Combustion Workshop*, NASA Lewis Research Center, 1993.
5. Friedman, R., Altenkirch, R., Pedley, M. and Torero, J.L., "Fire Safety", *Workshop on Research for Space Exploration: Physical sciences and processes Technology*, NASA/CP-1998-207431.
6. Ohlemiller, T.J. and Villa, K.M. "Material Flammability Test Assessment for Space Station Freedom," *NISTIR-4591*, National Institute of Standards and Technology, 1991.
7. Cordova, J.L., Ceamanos, J., Fernandez-Pello, A.C., Long, R.T., Torero, J.L. and Quintiere, J.G. "Flow Effects on the Flammability Diagrams of Solid Fuels," *Fourth International Micro-gravity Combustion Workshop*, NASA Lewis Research Center, 405-410, 1997.
8. Long, R.T, Torero, J.L., Quintiere, J.G. and Fernandez-Pello, A.C. "Scale and Transport Considerations on Piloted ignition of PMMA," *Sixth International Symposium on Fire Safety Science*, 1999.
9. Ivanov, A.V., Balashov, Ye. V., Andreeva, T.V. and Melikhov, A.S., "Experimental Verification of Material Flammability in Space," NASA/CR-1999-209405, November 1999.
10. Torero, J.L., Bahr, N.J. and Carman, E.J. "Assessment of Material Flammability for Micro-Gravity Environments" *48th International Astronautical Federation Congress*, Turin, Italy, *IAF-97-J.2.02*, October 1997.
11. Grayson, G., Sacksteder, K.R., Ferkul, P.V. and T'ien, J.S. "Flame Spreading Over a Thin Solid in Low-speed Concurrent Flow-Drop Tower Experimental Results and Comparison with Theory," *Microgravity Science and Technology*, VII/2, 187-195, 1994.
12. Ferkul, P.V. "A Model of Concurrent Flow Flame Spread Over a Thin Solid Fuel," NASA Contractor Report 191111, NASA Lewis Research Center, 1993.
13. Kasiwagi, T., Mell, W. E., McGrattan, K., Baum, H.R., Olson, S.L., Fujita, O., Kikuchi, M. and Ito, K. "Ignition, Transition, Flame Spread in Multidimensional Configurations in Microgravity," *Fourth International Micro-gravity Combustion Workshop*, NASA Lewis Research Center, 411-416, 1997.
14. T'ien, J.S. "The Possibility of a Reversal of Material Flammability Ranking from Normal Gravity to Microgravity," *Combustion and Flame*, 80, 355-357, 1990.
15. Quintiere, J.G., "A Simplified Theory for Generalizing Results from a Radiant Panel rate of Flame Spread Apparattus," *Fire and Materials*, Vol.5, No.2, 1981.

16. Quintiere, J. G. and Harkleroad, M., “New Concepts for Measuring Flame spread properties,” NBSIR-84-2943, National Bureau of Standards, 1984.
17. Wickman, I. S. "Theory of Opposed flame Spread," *Progress in Energy and Combustion Science*, **18**, **6**, pp. 553-593.
18. Janssens, M. L., “Thermal Model for Piloted Ignition of Wood Including Variable Thermophysical Properties,” *Fire Safety Science-3rd International Symposium*, 167-176, 1991.
19. Kashiwagi, T., “Effects of sample Orientation on Radiative Ignition,” *Combustion and Flame*, 44, 223-245, 1982.
20. Atreya, A., Carpenter, C., and Harkleroad, M., “The Effect of Sample Orientation on Piloted Ignition and Flame Spread,” *Fire Safety Science – 1st International Symposium*, p.97-109, 1985.
21. Hallman. J., “Ignition Characteristics of Plastics and Rubber,” Ph. D. Thesis, University of Oklahoma, Norman, OK, USA, 1971.
22. Steinhaus, T. “Evaluation of the Thermophysical Propertiesof Poly(Methylmethacrylate): A Reference Material for the Development of a Flammability Test for Micro-Gravity Environments,” M.S. Thesis, University of Maryland, 1999.
23. Mikkola, E., and Wichman, I.S., "On the Thermal Ignition of Combustible Materials," *Fire and Materials*, 14, pg. 1-10, 1989.
24. Atreya, A. "Ignition of Fires," *Phil. Trans. R. Soc. Lond.*, 356, 1998.
25. Roslon, M., Olenick, S., Walther, D., Torero, J.L., Fernandez-Pello, A.C. and Ross, H. D., “Microgravity Ignition Delay of Solid Fuels in Low Velocity Flow,” *AIAA-2000-0580*, 2000.
26. Orloff, L., De Ris, J. and Markstein, G.H. “Upward Turbulent Fire Spread and Burning of Fuel Surface,” *Fifteenth Symposium (International) on Combustion*, The Combustion Institute, 183-192, 1974.
27. Pagni P. J. and T. M. Shih, T.M., “Excess Pyrolyzate,” *Sixteenth Symposium (International) on Combustion*, The Combustion Institute, pp.1329, 1978.
28. Vietoris, T., Joulain, P. and Torero, J.L., “Experimental Observations on the Geometry and Stability of a Laminar Diffusion Flame in Micro-Gravity,” *Sixth International Symposium on Fire Safety Science,* 1999.
29. Fernandez-Pello, A.C. “The Solid Phase,” *Combustion Fundamentals of Fire*, G. Cox Editor, Academic Press, **2**, 31-100, 1995.
30. Emmons H. , The Film Combustion of Liquid Fuel, *Zeitschrift für Angewandte Mathematik und Mechanik*, Vol. 36, pp. 60, 1956.
31. Ferkul, P.V. and T’ien, J.S., “A Model of Low-Speed Concurrent Flow Flame Spread Over a Thin Fuel,” *Combustion Science and Technology*, 99, 345-370, 1994.
32. West, J., Tang, L., Altenkirch, R.A., Bhattacharjee, S., Sacksteder, K. and Delichatsios, M.A. “Quiescent Flame Spread over Thick Fuels in Micro-Gravity” *Twenty-sixth Symposium (International) on Combustion,* The Combustion Institute, 1335-1343, 1996.
33. Yang, C. T. and T’ien, J.S., “ Numerical Simulation of Combustion and Extinction of a Solid Cylinder in Low-Speed Cross Flow,” Journal of Heat Transfer, 120, 1055-1063, 1998.
34. Chen, H.C. and T’ien, J.S., “Diffusion Flame Stabilization at the Leading Edge of a Fuel Plate,” *Combustion Science and Technology*, 50, 283-306, 1986.
35. Vietoris, T. “Etude de la Combustion Quasi-Stationaire d’un Combustible Solid Soumis a un Ecoulement Parallele a sa Surface,” Ph.D. Thesis, University of Poitiers, France, 1999.
36. West, J., Tang, L., Altenkirch, R.A., Bhattacharjee, S., Sacksteder, K. and Delichatsios, M.A. “Quiescent Flame Spread over Thick Fuels in Micro-Gravity” *Twenty-sixth Symposium (International) on Combustion,* The Combustion Institute, 1335-1343, 1996.